Progress In Electromagnetics Research C, Vol. 72, 123–132, 2017

Application of Microwave Integrators for Interference Suppression

Lin-Chuan Tsai*

Abstract—In this study, a trapezoidal-rule integrator and inverting a differentiator are employed to form the transfer function of an approaching integrator in the Z domain. The integrator was implemented to verify the feasibility of the technique, and the integrator exhibited an operating frequency of 1.45 to 6 GHz. Adding microwave integrators to a receiver's radio frequency (RF) circuits in a communication link improves the signal-to-noise ratio (SNR). As a result, an experimental environment was constructed in a wireless local area network (WLAN) band (2400 to 2483.5 MHz). In addition, the RF transmitter emitted the main signal at 2.45 GHz, which included the high-frequency interfering signals at 3.5, 4.5, and 5.5 GHz. The integrators and low-pass filters were implemented to perform signal analysis of the RF signals. To compare the interference suppression of the integrators with the interference suppression of the original and low-pass filters, the receiving power of the main signal and the interfering signals from the different frequencies in the end of the receiver were analyzed. The experimental results indicated that inserting integrators into RF circuits improved the SNR of the communication link by up to 10 dB.

1. INTRODUCTION

Interference suppression issues have been extensively discussed in recent studies. To overcome the noise interference generated by communication circuits, many interesting interference suppression methods have been proposed [1–11]. In [1], joint suppression of two interferences was implemented in a receiver design based on the criterion of the minimum mean-squared error (MMSE). In [2], interference suppression was achieved through a zero-forcing algorithm that leveraged multichannel reception and requires channel state estimates for the interfering signal. Stochastic network structures have been used to demonstrate the average interference suppression performance. Several other interference suppression methods have been proposed [3–6].

Code-division multiple access (CDMA) for interference suppression has been examined [7–11]. In [7], an interference suppression technique was presented to use partial knowledge of spreading sequences to cancel a group of interfering signals. Knowledge of a complex scrambling sequence was used to project the desired signal away from the interference in the in-phase/quadrature (I/Q) complex plane. A novel low-complexity reduced-rank linear interference suppression technique was described and analyzed for direct-sequence (DS) CDMA systems based on the set-membership joint iterative optimization of received parameters [8]. Several other CDMAs have been proposed to suppress interference [11].

Many interesting discrete-time signal processing (DSP) techniques have been examined in the study of infinite impulse response (IIR) or finite impulse response (FIR) filter methods [12–16]. This paper indicates that the cascade line and two-section shunt-open elements of equal-electrical-length transmission lines can be expressed with a z variable in the discrete-time domain [17, 18]. Therefore,

Received 25 November 2016, Accepted 1 March 2017, Scheduled 20 March 2017
* Corresponding author: Lin-Chuan Tsai (ginggle@mail.lhu.edu.tw).
The author is with the Department of Electronic Engineering, Lunghwa University of Science and Technology, 300 Wanshou Rd., Sec. 1, Guishan Shiang, Taoyuan 33306, Taiwan, R.O.C.

the basic transmission-line elements can follow the transfer function of an integrator developed in the discrete-time domain. In particular, simple and accurate formulations are used to represent discrete-time IIR processes of a discrete-time integrator. To verify the theoretical study, the integrator was implemented in the microstrip format based on the physical length of each line section that had an operating frequency from 1.45 to 6 GHz. The experimental results, except for the results from the lower-frequency band, were similar to the theoretical values. The integrators were placed at the input port of the antenna in the receiver to accept the time integral of the received signals. This improved the weight of the binary message embedded in the modulated carrier signal. The experimental results indicated that inserting integrators into radio frequency (RF) circuits improved the signal-to-noise ratio (SNR) of the communication link by 7 dB. The experimental results further validated the proposed scheme. The integrators were simple and small, and thus could be practically implemented in communication circuits.

2. TRANSFER FUNCTIONS OF INTEGRATORS IN THE Z DOMAIN

Many methods have been created for proposing integrators using IIR or FIR techniques in DSP studies. The trapezoidal-rule integrator in the discrete-time domain is related to the complex-frequency variable, s^{-1}, as follows:

$$s^{-1} = H_1(z) = \frac{1 + z^{-1}}{c(1 - z^{-1})}, \tag{1}$$

where c is a real constant, and z^{-1} represents a unit of time delay. The trapezoidal-rule integrator in Eq. (1) represents a bilinear transformation of converting analog prototypes to discrete-time prototypes. In particular, a zero exists at $z = -1$ (normalized frequency, π). A z variable in Eq. (1) is replaced when the frequency domain response of the integrator is involved with the following relationship:

$$z = e^{j\Omega}, \tag{2}$$

where Ω is the frequency angle (or normalized frequency) and $0 \leq \Omega \leq \pi$. An integrator can also be obtained by inverting a differentiator, producing the following equation [17]:

$$H_2(z) = \frac{0.28 + 0.04648z^{-1}}{1 - z^{-1}}. \tag{3}$$

The amplitude responses of both Eqs. (1) and (3) as a function of normalized frequency are shown in Fig. 1. If $c = 5.56$ and $\Omega = 0.1\pi$, the amplitude responses of $H_1(z)$ are in a state of unity, and the maximal value of the transmission-line network's transmission coefficient is also in a state of unity. Fig. 1 also shows the amplitude response of an ideal integrator, which is inversely corresponding to the normalized frequency. Both Eqs. (1) and (3) deviate slightly from the value of an ideal integrator in the frequency band. To obtain an integrator that better fits the ideal integrator over the all normalized frequency bands, an approaching integrator is arranged as follows:

$$H_n(z) = 0.4 \cdot H_1(z) + 0.6 \cdot H_2(z) = \frac{0.24 + 0.0999z^{-1}}{(1 - z^{-1})}. \tag{4}$$

The frequency response of ideal integrators is

$$H_I(z) = \frac{1}{j\omega}. \tag{5}$$

The amplitude responses of both $H_n(z)$ and the ideal integrator are shown in Fig. 2. The transfer function of integrator $H_n(z)$ can represent the ideal integrator in the frequency band $(0 \leq \Omega \leq 0.6\pi)$. The integrators $H_n(z)$ become infinite at $\Omega = 0$. If the amplitude response must be complied in the low-frequency band, the integrator is difficult to implement at $\Omega = 0$. In particular, if an integrator is implemented by employing the integrator that is 1, $H_n(z)$ shows a value of 1 at the normalized frequencies 0.145π. To facilitate the design, the transmission lines were set, and the maximal value of the transfer function amplitude of transfer function $H_n(z)$ was set to 1 for the frequency range, $0 \leq \Omega \leq 0.145\pi$. The remaining part of the transfer function in the range $0.145\pi \leq \Omega \leq 0.6\pi$ satisfies

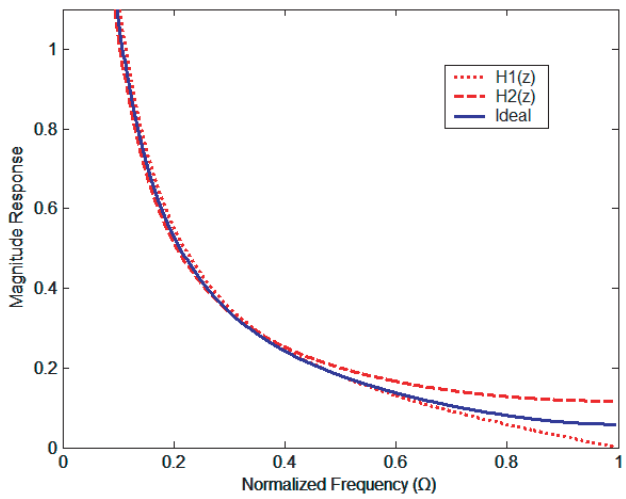

Figure 1. Amplitude responses of $H_1(z)$, $H_2(z)$, and ideal integrator.

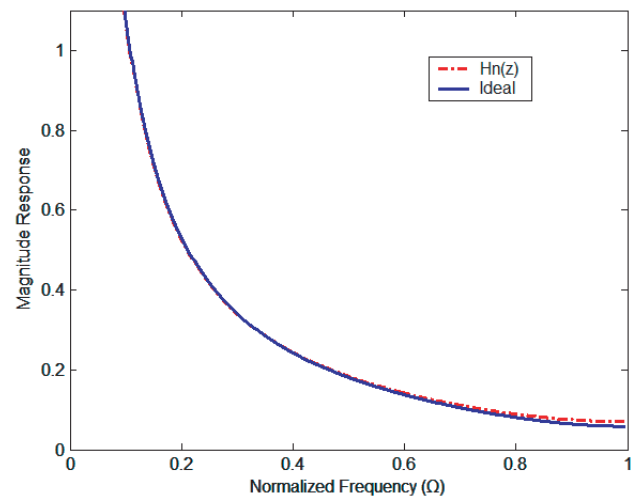

Figure 2. Amplitude responses of both $H_n(z)$ and ideal integrator.

Eq. (4). The circuit obtained in these circumstances behaves as an integrator of the frequency range, $0.145\pi \leq \Omega \leq 0.6\pi$. With such a condition, the integrator in Eq. (3) compensates for the zero occurring at the normalizing frequency ($\Omega = \pi$). The frequency changes over the entire band, as shown in Eq. (2), is equivalent to moving z variable along the unit circle, $|z| = 1$, in the complex Z plane. Equation (4) shows that a zero occurs at $z = -0.42$, and this zero is not possible by employing a transmission-line element. Zeroes happening on the unit circle, $|z| = 1$, can be implemented by employing two-section shunt-open elements. In addition, the zero at $z = -0.42$ is far away from the unit circle, and it has little effect on $H_n(z)$ in the entire frequency range, $0 \leq \Omega \leq \pi$. To implement an integrator, the next process is to obtain an equal-length transmission-line configuration, allowing its transmission coefficient to fit transfer function $H_n(z)$.

3. MEASUREMENT RESULTS

A two-port network is shown in Fig. 3, where $a(1)$ and $b(1)$ are the incident wave and reflected wave at port one, respectively, and $a(2)$ and $b(2)$ are the incident wave and reflected wave at port two, respectively. These waves are interrelated through the chain scattering parameters, T_{mn}, $(m, n = 1, 2)$, of a two-port network as follows:

$$\begin{bmatrix} a(1) \\ b(1) \end{bmatrix} = \begin{bmatrix} T_{11} & T_{12} \\ T_{21} & T_{22} \end{bmatrix} \begin{bmatrix} b(2) \\ a(2) \end{bmatrix}. \tag{6}$$

Figure 3. A two-port device.

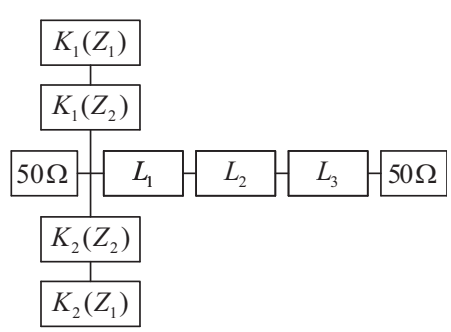

Figure 4. The configuration of a microwave integrator.

Table 1 shows basic transmission line element chain-scattering parameter matrices, T_{mn}, $(m, n = 1, 2)$, of a cascade line element and a two-section shunt-open element in the Z domain. The Z domain parameter is obtained by setting $z = e^{j\beta ili}$, where β_i is the propagation constant, and l_i is the physical length. Each cascade has $z^{(-1/2)}$ that gives a zero in z-domain when $z = 0$, and a two-section shunt-open element provides two zeros located on the unit circle. If a transmission line consists of K (K is positive integer) two-section shunt-open elements and L (L is positive integer) cascade line elements, then the matrix element $T_{11,\text{overall}}(z)$ of the overall circuit is denoted as follows:

$$T_{11,\text{overall}}(z) = \frac{\sum_{i=0}^{2K+L} d_i z^{-i}}{\prod_{k=1}^{K}\left(1 + 2\gamma_k z^{-1} + z^{-2}\right)\prod_{l=1}^{L} z^{-L/2}\left(1 - \Gamma_l^2\right)}. \tag{7}$$

Equation (7) shows that all d_i are real and are determined by the characteristic impedance of cascade line and two-section shunt-open elements. If the output of the serial circuit is appropriately terminated, we have $a(2) = 0$, and transfer function $T(z)$ of such a transmission line of serial circuit is obtained as follows:

$$T(z) = \frac{b(2)}{a(1)}\Big|_{a(2)=0} = \frac{1}{T_{11,\text{overall}}(z)} = z^{-L/2}\frac{\prod_{k=1}^{K=1}\left(1 + 2\gamma_k z^{-1} + z^{-2}\right)}{\sum_{i=0}^{2K+L} A_i z^{-i}}, \tag{8}$$

where $A_i = d_i/(\prod_{l=1}^{L}(1 - \Gamma_l^2))$ is a function of the characteristic impedances of two-section shunt-open elements and cascade-line elements. The term, $1 + 2z^{-1} + z^{-2}$, in the numerator in Eq. (8) is due to a two-section shunt-open element, and the term, $z^{-L/2}$, represents the delay factor of L cascade line elements.

Table 1. Basic transmission line elements chain-scattering parameter matrices.

	$\begin{bmatrix} T_{11} & T_{12} \\ T_{21} & T_{22} \end{bmatrix}$
cascade line 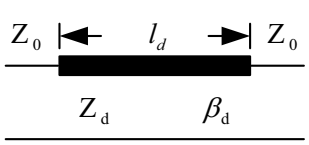	$\frac{1}{z^{-1/2}(1-\Gamma^2)}\begin{bmatrix} 1-\Gamma^2 z^{-1} & -(\Gamma - \Gamma z^{-1}) \\ \Gamma - \Gamma z^{-1} & -\Gamma^2 + z^{-1} \end{bmatrix}$ where $\Gamma = \frac{Z_d - Z_0}{Z_d + Z_0}$
two - section shunt - open 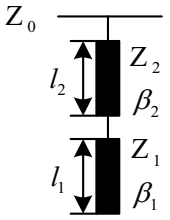	$\frac{1}{D(z)}\begin{bmatrix} \frac{2Z_2 D(z) - Z_0 C(z)}{2Z_2} & \frac{Z_0 C(z)}{2Z_2} \\ -\frac{Z_0 C(z)}{2Z_2} & \frac{2Z_2 D(z) - Z_0 C(z)}{2Z_2} \end{bmatrix}$ where $C(z) = 1 - z^{-2}$, $D(z) = 1 - 2\gamma z^{-1} - z^{-2}$, $\gamma = \frac{Z_1 - Z_2}{Z_1 - Z_2}$

To reduce the circuit size and perform the optimization, it might be easier to synthesize the integrator circuit if two-section shunt-open stubs were used than the minimal requirement of the discrete-time integrator. The synthesis algorithm step transforms both $T(z)$ and $H_n(z)$ into whole new forms. The operation in this step divides both $T(z)$ and $H_n(z)$ by the terms, producing $T(z)$ zeroes on the unit circle in the Z plane. In other words, the $T(z)$ numerator that produces the unit-circle zeroes is removed from $T(z)$ and appears in the denominator of $H_n(z)$. It might be easier to synthesize the integrator network if two-section shunt-open elements were used than that the minimal requirement of the discrete-time integrator was used. To implement the integrator with cascade line and two-section shunt-open elements, the electrical length of each element was set to 90° at the normalized frequency. In this investigation, to construct microwave integrators, microstrip lines were used to follow transmission line elements. The microstrip lines were assumed to be both dispersionless and lossless for the present study. Because of the restrictions of the obtainable manufacturing method, the line widths of the cascade line and the two-section shunt-open elements were confined to 0.1 mm. Therefore, the largest value of all characteristic impedances of transmission line elements was confined to 160 Ω. Under such circumstances, one two-section hunt-open element, as well as a cascade line element, may be selected as the basic circuit. The next process is to match the coefficients of the denominators in Eq. (8), ensuring that $T(z)$ is as close to $H_n(z)$ as possible. In Eq. (8), A_i is decided by the characteristic impedance of all transmission line elements. By using the optimization process [19–21], the values of the characteristic impedances of the transmission lines are adjusted according to the goal that the difference between Eqs. (4) and (8) is minimized in the sense of mean square error (MSE). The optimization algorithm showed that $K = 2$ and $L = 3$ when the characteristic impedances of transmission lines were obtained. The illustration of the circuit used to synthesize th integrator is shown in Fig. 4. Fig. 5 shows the frequency responses of $T(z)$ and $H_n(z)$. Microstrips were used to implement the integrator. Fig. 6 shows the photograph of the microwave integrator, which was built on an RT/Duroid RO4003C substrate with a dielectric constant of $\varepsilon_r = 3.55$, loss tangent of $\tan\delta = 0.0025$, and thickness of 1.524 mm. The total length of the integrator, excluding the 50-Ω reference lines on both sides, was 19.65 mm. The characteristic impedances of the cascade line elements were $L_1 = 130\,\Omega$, $L_2 = 102\,\Omega$, and $L_3 = 106\,\Omega$, and the two two-section shunt-open elements were $K_1(Z_2) = 22\,\Omega$, $K_1(Z_1) = 154\,\Omega$, $K_2(Z_2) = 22\,\Omega$, and $K_2(Z_1) = 154\,\Omega$.

Figure 7 shows the measured and simulated results $S_{21}(f)$ and $S_{11}(f)$ of the integrators shown in Fig. 6. The slight difference between the experimental results and the theoretical ones is due to conductor loss, dielectric loss, as well as the restriction of manufacturing. The experimental results of the circuit in Fig. 6 fit the theoretical values for the frequency range, 1.45 GHz $\leq f \leq$ 6 GHz. As

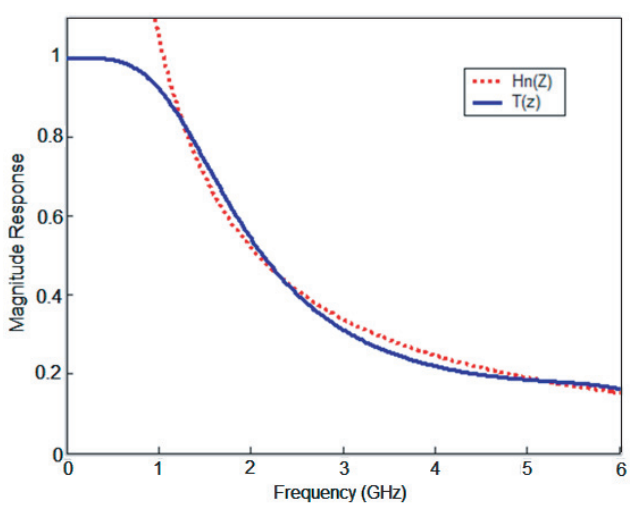

Figure 5. The magnitude function of $H_n(z)$ and the magnitude function $T(z)$ of the microwave integrator.

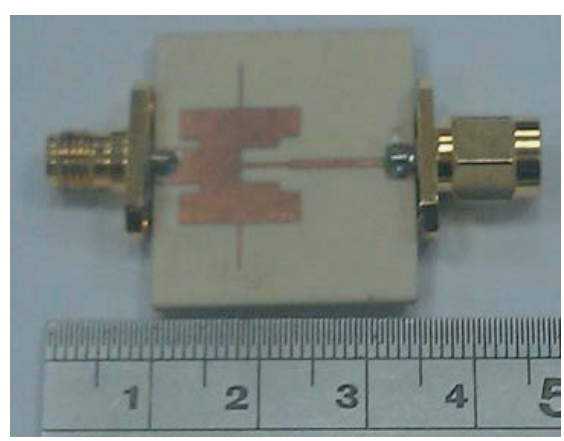

Figure 6. Physical layout of the microwave integrator.

mentioned in the previous section, the magnitude of $S_{21}(f)$ exhibits a value of unity for the frequency range, $0\,\text{GHz} \leq f \leq 1\,\text{Hz}$. Therefore, the circuit in Fig. 6 behaves as an integrator for the frequency band, $1.45\,\text{GHz} \leq f \leq 6\,\text{GHz}$. The experimental results are still in good agreement with the theoretical values. The integrator is a low-pass filter with close frequency dependence. To demonstrate the interference suppression of the difference between the integrator and the conventional low-pass filter, a three-order Butterworth low-pass filter was fabricated. Fig. 8 shows a photograph of the low-pass filter that was built on the same substrate as the above mention. Fig. 9 shows the measured and simulated results of $S_{21}(f)$ and $S_{11}(f)$ for the low-pass filter. Notably, both the Butterworth low-pass filter in Fig. 8 and the microwave integrator in Fig. 6 have the -3-dB point at the same frequency in the attenuation band. In addition, a three-order Butterworth low-pass filter distinguishes the magnitude responses of $S_{21}(f)$ from the microwave integrator at higher frequencies. To show the impedance profiles of a conventional low-pass filter, a Butterworth low-pass filter was constructed. The attenuation band of the filter was $-3\,\text{dB}$ at $1.45\,\text{GHz}$ and $-10\,\text{dB}$ at $2.85\,\text{GHz}$. The filter impedance profiles of a three-section line were constructed as 23, 150, and $23\,\Omega$, excluding the reference lines on both sides, which was 34.13 mm. To compare the interference suppression of the integrators, original, and low-pass filter, the receiving power

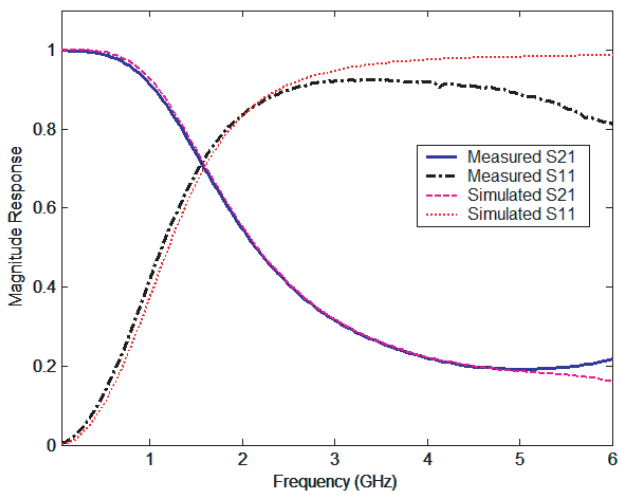

Figure 7. Measured and simulated results of $S_{21}(f)$ and $S_{11}(f)$ for a microwave integrator.

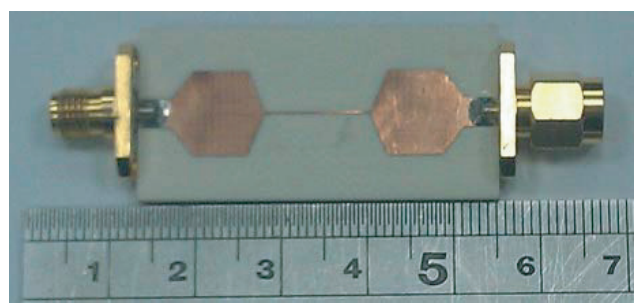

Figure 8. Physical layout of the low-pass filter.

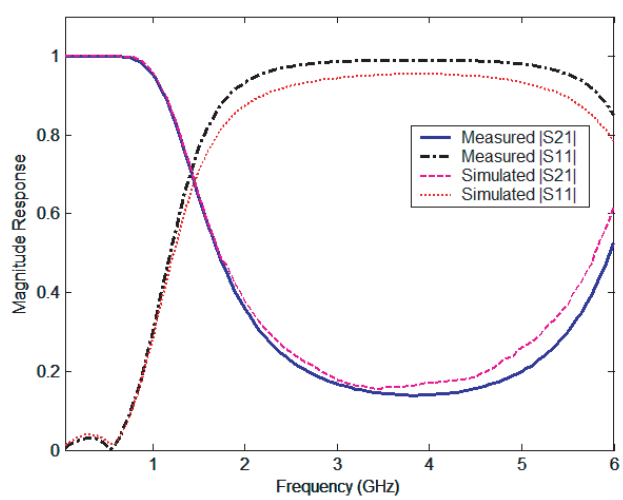

Figure 9. Measured and simulated results of $S_{21}(f)$ and $S_{11}(f)$ for the low-pass filter.

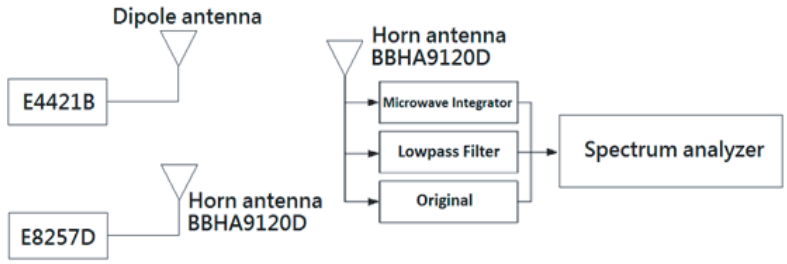

Figure 10. Experimental environment of SNR improvement.

Figure 11. Photograph of experimental environment.

of the main signals and interfering signals of the different frequencies in the end of the receiver were analyzed. Fig. 10 shows the experimental environment for the transmitter and receiver. To examine the integrator efficiency of the receiver SNR in the communication system, an experimental environment was built. In the case of the transmitter, an Agilent E4421B was employed to generate the main signal, transmitted by a dipole antenna at 2.45 GHz, which was built from the same substrate as that mentioned, and the antenna gain is approximately 3 dBi. In addition, an Agilent E8257D generated a CW Gaussian noise interfering signal at 3.5, 4.5, and 5.5 GHz, transmitted by a BBHA9120D horn antenna. In the receiver, a BBHA9120D horn antenna was used to receive the main and interfering signals in serial from the integrator and conventional low-pass filter. A photograph of the experimental environment is shown in Fig. 11. In the case of channels with many fast fading cycles, the path loss applies to the power averaged over several fading cycles. These can be constructed by applying a link budget [22]:

$$P_R = \frac{P_T G_T G_R}{L_T L L_R} \tag{9}$$

where P_T is the transmitted power, P_R the received power, G_T the antenna gain for the transmitter, G_T the antenna gain for the receiver, L_T the feeder loss of the transmitter, L_R the feeder loss of the receiver, and L the path loss. The BBHA9120D horn antenna gain is approximately 20 dBi, and the feeder losses of the transmitter and receiver are approximately 6 dB. For the radio wave propagation, the free space path loss model [23] is expressed as

$$L = 32.44 + 20\log_{10}(d) + 20\log_{10}(f), \tag{10}$$

where $20\log_{10}(d)$ is the free space path loss referenced to 1 m, and f is the frequency in GHz. Under such channel conditions, other interference signals (such as Bluetooth, ZigBee, and WLAN) were neglected. Hence, the path loss from Eq. (10) is 92.44 dB. For example, P_R is equal to -28.44 dBm when P_T is set at 1 W.

The original, integrator, and low-pass filter signals were analyzed by an E4408B spectrum analyzer, and the SNR improvement was calculated by dealing with the receiving power. At the receiver end, the original is the measured result without adding an integrator or low-pass filter. Input SNR, output SNR, and SNR improvement are expressed in Eqs. (11), (12), and (13), respectively [6]:

$$\text{SNR at the input} = 10\log_{10}\frac{E\left(s_k^2\right)}{E\left(|z_k - s_k|^2\right)} \tag{11}$$

$$\text{SNR at the output} = 10\log_{10}\frac{E\left(s_k^2\right)}{E\left(\varepsilon_k - s_k|^2\right)} \tag{12}$$

$$\text{SNR improvement} = 10\log_{10}\frac{E\left(|z_k - s_k|^2\right)}{E\left(|\varepsilon_k - s_k|^2\right)}, \tag{13}$$

where s_k is the power of the main signal, z_k the power of the interfering signal, and ε_k the output signals of the integrator and low-pass filter signals. For example, the input signal-to-noise-and-interference ratio

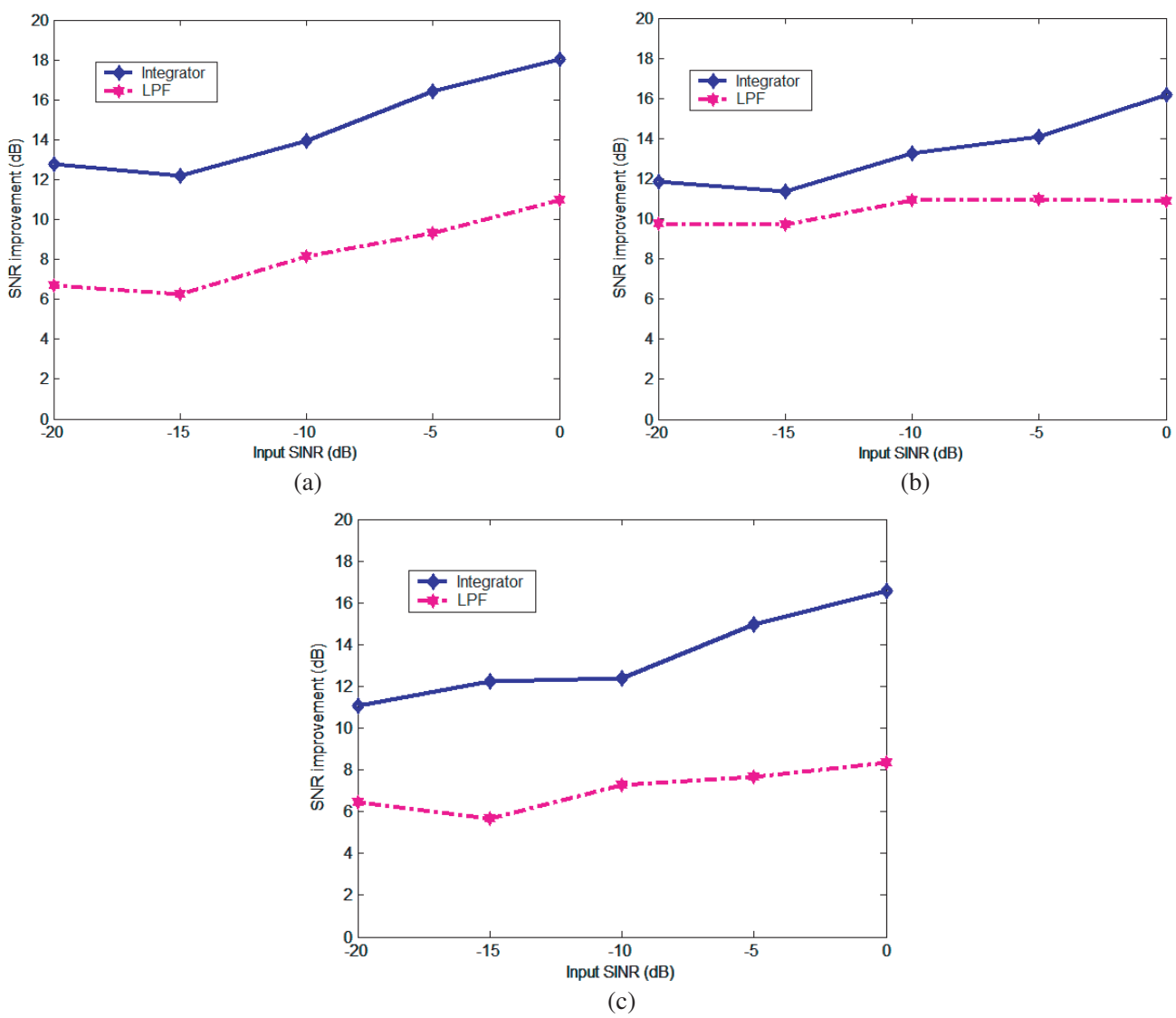

Figure 12. (a) SNR improvement for the integrator at interfering signal 3.5 GHz. (b) SNR improvement for the integrator at interfering signal 4.5 GHz. (c) SNR improvement for the integrator at interfering signal 5.5 GHz.

(SINR) is equal to 0 dB when the main signal power is set at 0.5 W, and the interfering signal is set at 3 mW. In the receiver, the theoretical values of the main signal strength and interfering signal strength are −43.45 dBm and −43.66 dBm, respectively. The experimental procedure required the transmitted frequency of the main signal to be set at an FM modulation of 2.45 GHz with a fixed constant power by changing the frequency and the interfering signal power, and calculating the SNR improvement by using Eq. (13). Figs. 12(a), (b), and (c) show the results produced by the previously described experimental environment. Fig. 12(a) shows the measured results for some of the cases. The measured results indicated that the integrator improved the SNR by 7.07 dB for the low-pass filter when the input signal-to-noise-and-interference ratio (SINR) was 0 dB at 3.5 GHz. The integrator improved the SNR more than the low-pass filter in all cases. The integrator exhibited its optimal performance when rejecting interference in certain conditions. For instance, the experimental results demonstrated that the integrator improved the SNR by up to 8.23 dB for the low-pass filter when the input SINR was 0 dB at 5.5 GHz. However, in certain conditions, the integrator improved the SNR by only 2 to 3 dB more than the low-pass filter. The integrator exhibited this poor performance because the input SINR power was −20 dB; the power of the main and interfering signals was weak; the integrator had a poor ability to distinguish the main and interfering signals. In addition, the low-pass filter performance was inferior to the integrator performance at 5.5 GHz because the low-pass filter generated amplitude responses with periodic properties, which repeated a period at 6.77 GHz. As a result, the integrator improved the SNR more than the low-pass filter at higher-frequency ranges. Furthermore, when the input SNR was 0 dB at 5.5 GHz, the integrator improved the SNR by 8.23 dB more than the low-pass filter. Compared with different input SINR frequencies, the SNR improvement difference between the integrator and original increased by up to 5.22 dB at 3.5 GHz and 7.19 dB at 4.5 GHz.

4. CONCLUSION

This paper presents a microwave integrator based on microstrip transmission lines. In particular, the Z domain representations of scattering characteristics of equal-length nonuniform transmission lines facilitated the implementation of discrete-domain integrators in the microwave frequency range. To compare the interference suppression of the integrators, original, and low-pass filter, the receiving power of the main signals and the interfering signal of the different frequencies in the end of the receiver were analyzed. Microwave integrators and low-pass filters in the same experimental environment demonstrated that the microwave integrator signals improved the SNR better than the low-pass filter by more than approximately 6 dB. The integrators generated the highest 8.23 dB SNR improvement when the input SINR was 0 dB at 5.5 GHz. The main reason for this result is that the microwave integrators should be able to keep the main signal while filtering out high-frequency interfering signals. As a result, the microwave integrator increases the signal sensitivity of the receiver, improving the quality of the received signal. The experimental results indicate that microwave integrators can improve a communication link SNR.

ACKNOWLEDGMENT

This work was supported by the National Science Council, R.O.C., under Grant NSC 103-2221-E-262-003.

REFERENCES

1. He, J., G. Gu, and Z. Wu, "MMSE interference suppression in MIMO frequency selective and time-varying fading channels," *IEEE Trans. Signal Processing*, Vol. 56, No. 8, 3638–3651, Aug. 2008.
2. Sun, Y. and T. Pratt, "Narrowband PLC SIMO-based interference suppression with zero-forcing," *IEEE Power Deliv.*, Vol. 28, No. 4, 2022–2029, Apr. 2013.
3. Gupta, A. S. and A. Singer, "Interference suppression for memoryless nonlinear multiuser systems using constellation structure," *IEEE Trans. Signal Processing*, Vol. 56, No. 11, 5589–5604, Nov. 2008.

4. Zhou, H. and B. Wen, "Radio frequency interference suppression in small-aperture high-frequency radars," *IEEE Geo. Remote Sensing Lett.*, Vol. 9, No. 4, 788–792, Apr. 2012.
5. Perez-Solano, J. J., S. Felici-Castell, and M. A. Rodriguez-Hernandez, "Narrowband interference suppression in frequency-hopping spread spectrum using undecimated wavelet packet transform," *IEEE Trans. Vehicular Tech.*, Vol. 57, No. 3, 1620–1629, Mar. 2008.
6. Talmon, R., I. Cohen, and S. Gannot, "Single-channel transient interference suppression with diffusion maps," *IEEE Trans. Audio, Speech, and Language Processing*, Vol. 21, No. 1, 132–144, Jan. 2013.
7. Bottomley, G. E., "CDMA downlink interference suppression using I/Q projection," *IEEE Trans. Wireless Comm.*, Vol. 2, No. 5, 890–900, May 2003.
8. Clarke, P. and R. C. de Lamare, "Low-complexity reduced-rank linear interference suppression based on set-membership joint iterative optimization for DS-CDMA systems," *IEEE Trans. Vehicular Tech.*, Vol. 60, No. 9, 4324–4337, Sept. 2011.
9. De Lamare, R. C. and P. S. R. Diniz, "Blind adaptive interference suppression based on set-membership constrained constant-modulus algorithms with dynamic bounds," *IEEE Trans. Signal Processing*, Vol. 61, No. 5, 1288–1301, May 2013.
10. Hombs, B. and J. S. Lehnert, "Multiple-access interference suppression for MC-CDMA by frequency-domain oversampling," *IEEE Trans. Comm.*, Vol. 53, No. 4, 677–686, Apr. 2005.
11. Glisic, S. G., Z. B. Nikolic, B. Dimitrijevic, and G. K. Woodward, "Multilayer LMS interference suppression algorithms for CDMA wireless network," *IEEE Trans. Comm.*, Vol. 48, No. 8, 1413–1422, Aug. 2000.
12. Al-Alaoui, M. A., "Novel IIR differentiator from the Simpson rule," *IEEE Trans. Circuits Systems — I*, Vol. 41, No. 2, 186–187, Feb. 1994.
13. Tseng, C.-C., "Design of fractional order digital FIR differentiators," *IEEE Signal Processing Letters*, Vol. 8, No. 3, 77–79, Mar. 2001.
14. Kumar, B. and S. C. Dutta-Roy, "Design of digital differentiators for low-frequencies," *Proc. IEEE*, Vol. 76, No. 3, 287–289, Mar. 1988.
15. Pei, S. C. and J. J. Shyu, "Analytic closed form matrix for designing high order digital differentiators using eigenapproach," *IEEE Trans. Signal Processing*, Vol. 44, No. 3, 698–701, Mar. 1996.
16. Al-Alaoui, M. A., "A class of second-order integrators and low-pass differentiators," *IEEE Trans. Circuits Systems — I*, Vol. 42, No. 4, 220–223, Apr. 1995.
17. Hsue, C.-W. L.-C. Tsai, and K.-L. Chen, "Implementation of first-order and second-order microwave differentiators," *IEEE Trans. Microwave Theory Tech.*, Vol. 52, No. 5, 1443–1448, May 2004.
18. Oppenheim, A. V. and R. W. Schafer, *Discrete-time Signal Processing*, Prentice-Hall, Englewood Cliffs, NJ, 1998.
19. Tsai, L. C. and C. W. Hsue, "Dualband bandpass filter using equal length coupled serial shunted lines and Z-domain technique," *IEEE Trans. Microwave Theory Tech.*, Vol. 52, No. 4, 1111–1117, Apr. 2004.
20. Chang, D.-C. and C.-W. Hsue, "Design and implementation of filters using transfer functions in the Z domain," *IEEE Trans. Microwave Theory Tech.*, Vol. 49, No. 5, 979–985, May 2001.
21. Chang, D.-C. and C.-W. Hsue, "Wide-band equal-ripple filters in nonuniform transmission lines," *IEEE Trans. Microwave Theory Tech.*, Vol. 50, No. 4, 1114–1119, Apr. 2002.
22. Loyka, S. and A. Kouki, "Using two ray multipath model for microwave link budget analysis," *IEEE Antennas and Propagation Magazine*, Vol. 43, No. 5, 31–36, Oct. 2001.
23. Parsons, J. D., *The Mobile Radio Propagation Channel*, 2nd edition, Wiley, New York, 2000.